Age dependent changes in synaptic NMDA receptor composition in adult human cortical neurons.

Pegasiou C.M. [1,2], Zolnourian A.[3,4], Gomez-Nicola D. [1], Deinhardt, K. [1], Nicoll J.A.R.[2, 5], Ahmed A.I. [3,4], Vajramani G. [3], Grundy P. [3], Verhoog, M.B.[6,7], Mansvelder, H.D.[6], Perry V.H.[1,8], Bulters D. [3,4], Vargas-Caballero M. [1,2]

Author affiliations

[1]School of Biological Sciences, University of Southampton

[2]Institute for Life Sciences, University of Southampton.

[3]Department of Neurosurgery, University Hospital Southampton, Wessex Neurological Centre.

[4]Clinical Neurosciences, Clinical and Experimental Sciences, Faculty of Medicine, University of Southampton UK

[5]Department of Cellular Pathology, University Hospital Southampton NHS Foundation Trust, Southampton, UK

[6]Department of Integrative Neurophysiology, Center for Neurogenomics and Cognitive Research, Neuroscience Amsterdam, VU University Amsterdam, The Netherlands

[7]Present address: Division of Cell Biology, Department of Human Biology, Neuroscience Institute, Faculty of Health Sciences, University of Cape Town, Cape Town, South Africa

Corresponding author:

Dr. Mariana Vargas-Caballero

Abstract

The molecular processes underlying the ageing-related decline in cognitive performance and memory observed in humans are poorly understood. Studies in rodents have shown a decrease in N-methyl-D-aspartate receptors (NMDARs) that contain the GluN2B subunit in ageing synapses, and this decrease is correlated with impaired memory functions. However, the age-dependent contribution of GluN2B containing receptors to synaptic transmission in human cortical synapses has not been previously studied. We investigated the synaptic contribution of GluN2A and GluN2B containing NMDARs in adult human neurons using fresh non-pathological temporal cortical tissue resected during neurosurgical procedures. The tissue we obtained fulfilled quality criteria by the absence of inflammation markers and proteomic degradation. We show an age-dependent decline in the NMDA/AMPA receptor ratio in adult human temporal cortical synapses. We demonstrate that GluN2B containing NMDA receptors contribute to synaptic responses in the adult human brain with a reduced contribution in older individuals. With previous evidence demonstrating the critical role of synaptic GluN2B in regulating synaptic strength and memory storage in mice, this progressive reduction of GluN2B in the human brain during ageing may underlie a molecular mechanism in the age-related decline in cognitive abilities and memory observed in humans.

Introduction

Glutamate is the neurotransmitter of cortical and hippocampal pyramidal neurons and thus is a mediator cognitive functions. Glutamate-gated receptors of the NMDA subtype require intracellular depolarisation to relieve voltage-dependent extracellular Mg^{2+} block of the ion channel pore. Once opened, NMDAR channels can allow Ca^{2+} influx which triggers the synaptic plasticity processes thought to support many forms of learning and memory (Bliss and

48 Collingridge, 1993; Takeuchi et al. 2013). NMDARs are tetrameric ion channels containing 2
49 GluN1 (obligatory) subunits and 2 GluN2 subunits, which in the adult forebrain most commonly
50 comprise GluN2A and GluN2B. In addition to well characterised di-heteromers (GluN1/GluN2A or
51 GluN1/GluN2B) (reviewed in Paoletti et al. 2013), tri-heteromeric forms (GluN1/GluN2A/GluN2B)
52 have been selectively studied in expression systems (Hansen et al. 2014) and there is
53 electrophysiological and biochemical evidence for NMDAR tri-heteromers and adult rodent brain
54 (Al-Hallaq et al 2007; Rauner and Köhr, 2011; Stroebel et al. 2018). Furthermore, a short
55 primate-specific GluN2A isoform (GluN2A-S) forms functional NMDAR together with GluN1 and
56 accounts for one third of the total GluN2A protein in adult human cortex (Warming et al. 2019).
57
58 The subunit composition of NMDA receptors (NMDARs) determines their ion channel properties
59 (Vicini et al. 1998), and protein-protein interactions with downstream molecular cascades that
60 are linked to plasticity, survival and excitotoxicity (Hardingham and Bading, 2010; Lussier et al.
61 2015). Synaptic localisation of distinct NMDAR subunits is highly regulated by neurons and
62 undergoes marked developmental changes in rodent neocortex with a switch from GluN2B to
63 GluN2A rich synapses postnatally (Dumas, 2005; Mierau et al. 2004; Yashiro and Philpot, 2009).
64 In adult synapses, a fraction of GluN2B-containing NMDARs is maintained in a highly regional-
65 specific manner; sensory and association cortices maintain a lower proportion of GluN2B
66 containing NMDARs than hippocampal and prefrontal cortex areas (Mierau et al. 2004; Wang et
67 al. 2008; Kohl et al. 2011).
68
69 Previous research using human post-mortem tissue has shown that the ratio of *GRIN2B*/*GRIN2A*
70 mRNA undergoes a reduction during early development similar to that found in many other
71 species (Bar-Shira et al. 2015; Bagasrawala et al. 2016) and this is also evident at the protein

72 level with an age-dependent reduction in GluN2B, and an increase in GluN2A, in the first years of
73 life (Jantzie et al. 2013). Importantly, GluN2B has been found to co-assemble with PSD-95 in
74 resected brain tissue from patients <17 years old (Ying et al. 2004), suggesting that GluN2B
75 might contribute to synaptic transmission in young adult cortical synapses. However, it is
76 unknown whether there is further reduction of GluN2B in adulthood or old age and whether
77 GluN2B-containing NMDAR contribute to synaptic transmission in the adult brain.
78
79 Here, we tested directly whether GluN2B-containing NMDARs contribute to synaptic function in
80 adult human cortical neurons. We used non-pathological tissue resected during neurosurgery
81 from patients to test for NMDAR subunit composition in tissue homogenates and their
82 association with the major synaptic scaffolding protein PSD-95. Furthermore we analysed
83 synaptic transmission using patch clamp electrophysiology in brain slices of live temporal cortex.
84 Our results show that NMDA/AMPA ratio decreases with age with a marked decline of GluN2B-
85 NMDAR current in older synapses.
86
87 Materials and Methods
88 Tissue Collection
89 The use of human tissue complied with the Human Tissue Act (Southampton Research
90 Biorepository study reference number: SRB002/14). Informed consent was obtained from all
91 patients to use surgically-resected tissue not required for diagnostic purposes. Temporal cortex
92 was chosen as its availability was sufficient to allow statistical analysis of data. Human brain
93 slices were prepared as previously described by Verhoog et al. (2013). Briefly, resected tissue
94 was obtained from temporal cortex of patients undergoing surgery for the removal of deeper
95 structures. We obtained temporal cortical tissue from 17 individual neurosurgery cases (Table 1).

96 In all cases, resected neocortical tissue was located well outside the epileptic focus or tumour
97 and displayed no structural abnormalities in preoperative magnetic resonance imaging
98 investigations (Fig 1A). The tissue collected was identified as macroscopically normal at the time
99 of collection by the operating team. The tissue was immediately placed in ice-cold artificial

Case Number	Sex	Age	Diagnosis	Medication prescribed (time with medication)	Other medical history	Brain area
0001	M	49	Hippocampal sclerosis	Carbamazepine (>1 year)	None known	Right temporal lobe
0004	M	52	Hippocampal sclerosis	Lamotrigine, Clobazam (>1 year)	None known	Right temporal lobe
0005	F	60	Hippocampal sclerosis	Levetiracetam, Phenytoin, Amitriptyline, Citalopram, Morphine, Omeprazole, Mebeverine (>1 year)	None known	Right anterior temporal lobe
0007	F	21	DNET	Lamotrigine, Eslicarbazepine (>1 year), Dexamethasone, Omeprazole	None known	Left anterior temporal lobe
0008	M	71	Glioblastoma	Phenytoin, Alfuzosin, Allopurinol, Dexamethasone, Paracetamol, Lansoprazole (<3 months)	None known	Right anterior temporal lobe
0010	M	28	Hippocampal sclerosis	Lamotrigine, Clobazam, Carbamazepine (>1 year)	None known	Right posterior lateral temporal lobe (inferior temporal gyrus)
0011	F	42	Glioma	N/A	None known	Left anterior temporal cortex
0014	M	32	Hippocampal sclerosis	Lamotrigine, Levetiracetam, Pregabalin, Citalopram, Paracetamol, Salbutamol (>1 year)	Asthma, Depression	Right anterior temporal lobe
0016	F	36	Hippocampal sclerosis	Gabapentin, Lamotrigine, Citalopram, Senna, Omeprazole, Paracetamol (>1 year)	None known	Left anterior temporal lobe
0017	F	62	Hippocampal sclerosis	Lamotrigine, Carbamazepine, , Diazepam, Pregabalin, Citalopram Prochlorperazine (>1 year)	Depression, Hypertension, Gastroreflux disease	Right anterior temporal lobe
0018	M	30	Cavernous malformation	Lamotrigine, Levetiracetam (>1 year)	None known	Right anterior temporal lobe
0020	F	70	Arteriovenous malformation	Fentanyl Patch, Paracetamol, Amlodipine, Omeprazole, Estradiol, Avastatin, Qvar 100, Colecalciferol, Prednisolone, Nitrofurantoin (<1 month)	Hysterectomy, Urostomy, Acute Myocardial Infarction, Hypertension, Polymyalgia Rheumatica, Hypercholesterolaemia, Recurrent Urinary Tract Infections	Right lateral temporal lobe (middle temporal gyrus)
0021	M	49	Hippocampal sclerosis	Carbamazepine, Atenolol (>1 year)	Glandular Fever	Left posterior temporal lobe
0022	F	58	Intracerebral and subarachnoid haemorrhage	Dihydrocodeine, Nimodipine, Paracetamol (N/A)	Multiple Aneurysms	Right anterior temporal lobe
0024	F	50	Cavernous malformation	Lamotrigine, Ibuprofen, Paracetamol (>1 year)	Gall stones, Hysterectomy	Right lateral temporal lobe (superior temporal gyrus)
0026	M	27	Mesial temporal DNET with signal changes in the hippocampus	Carbamazepine, Clobazam, Levetiracetam, Zonisamide, Morphine, Dihydrocodeine, Dexamethasone, Omeprazole, Paracetamol, Colecalciferol (>1 year)	None known	Right anterior temporal lobe
0028	F	38	Epilepsy	Zopiclone, Amitripyline, Zonisamide, Citalopram, Zafirlukast, Cinnarizine, Loestrin (>1 year), Senna	Asthma	Right anterior temporal lobe

100

101 **Table 1. Human tissue case data.** F, female; M, male. Pathological tissue from patients 0011

102 and 0021 were used as positive control in Fig 1D. Cases that met exclusion criteria: cases 8

103 and 20 (Iba1 quantification), and case 11 (GluN2B cleavage). DNET, Dysembryoplastic

104 neuroepithelial tumour.

105

106

107 cerebrospinal fluid (ACSF) solution while still in theatre. ACSF contained the following (in

108 mM): 110 choline chloride; 26 $NaHCO_3$; 10 D-glucose; 11.6 sodium ascorbate; 7 $MgCl_2$; 3.1

109 Sodium pyruvate; 2.5 KCl; 1.25 $NaH_2PO_4.2H_2O$; 0.5 $CaCl_2$. Tissue was then taken to the

110 laboratory and fresh frozen for biochemistry, fixed for immunohistochemistry or processed

111 for slice electrophysiology. Transfer time between operating theatre and laboratory was

112 approximately of 10-15 minutes.

113

114 Animal care and experimental procedures were conducted in accordance with UK Home Office

115 regulations under the Animals (Scientific Procedures) Act of 1986. Mice were decapitated

116 following isoflurane anaesthesia. Brains were extracted in ice-cold ACSF and sliced or snap-

117 frozen. All brain tissue samples were stored in the -80°C freezer until lysed.

118

119 Acute Brain Slice Preparation

120 Brain slices (350 μm thick) were prepared in ice-cold choline ACSF solution (Verhoog et al. 2013)

121 using a Campden Instruments vibrating microtome and kept for 30 min at 35-37°C, then at room

122 temperature in recording ACSF containing the following (in mM): 126 NaCl; 2 $CaCl_2$; 10 glucose;

123 2 $MgSO_4.7H_2O$; 3 KCl; 1.25 $NaH_2PO_4.2H_2O$; 26.4 $NaHCO_3$; pH 7.2-7.4. The ACSF was bubbled
124 with carbogen gas (95% O_2/5% CO_2) and had an osmolarity of ~300 mOsm.
125
126 Electrophysiological Recordings
127 Following previously published methods (Verhoog et al. 2013), slices were transferred to a
128 submerged-style recording chamber and superfused with recording ACSF at a rate of
129 ~1.5ml/min. Whole-cell voltage clamp recordings were performed using glass pipettes (4-6 MΩ)
130 pulled from borosilicate glass, yielding a series resistance of 10-20 MΩ. Recordings were made at
131 room temperature (21-25°C) using Cs-gluconate-based intracellular solution, containing (in mM):
132 70 Gluconic acid; 10 CsCl; 5 NaCl; 10 BAPTA free acid; 10 Hepes; 10 QX-314; 0.3 GTP; 4 Mg-ATP;
133 pH was titrated to 7.25 with CsOH. The estimated final Cs concentration for the intracellular
134 solution was 120 mM. The final osmolarity was 280 ± 5 mOsmol-1. All voltage values were
135 corrected for the liquid junction potential of -15 mV which was measured directly. Biocytin
136 (2mg/ml) was added for labelling (Fig 1C) and following recordings, the slice was fixed in 4%
137 paraformaldehyde for 24 hours and stored in PB. Slices were washed in 0.1M PB, dehydrated
138 using increasing ethanol percentages (70%, 80%, 95% and 2x100%, for 5 minutes each) and then
139 processed using an avidin–biotin–peroxidase kit (Vector laboratories).
140
141 Excitatory postsynaptic currents (EPSCs) were evoked using a stimulus isolator unit (ISO-Flex,
142 A.M.P.I.) connected to a monopolar extracellular stainless-steel electrode, which was placed
143 near an apical dendrite and within 100-150 µm from a LII-III pyramidal neuron soma. Stimulation
144 strength was adjusted to yield a ~200 pA EPSC amplitude at a holding potential of −70 mV to
145 minimise space-clamp error. Synaptic stimulation was evoked at 0.07 Hz with 100 µs stimulus
146 length. Series resistance was not compensated during recordings but was monitored before each

147 stimulation with a 5 mV 50 ms step pulse. Recordings were terminated if series resistance
148 changed by more than 20%. Data were low-pass filtered at 2 kHz and acquired at 20 kHz with an
149 Axon Multiclamp 700B amplifier (Molecular Devices, Sunnyvale, U.S.A.) using MATLAB
150 (Mathworks, Natick, U.S.A.) and custom software (MatDAQ, Hugh P.C. Robinson, University of
151 Cambridge 1995-2013). EPSCs were recorded 10 minutes after initiating a whole-cell patch to
152 allow the dialysis of the Cs-based internal solution. EPSCs were recorded in the presence of
153 gabazine (also known as SR-95531, Tocris Bioscience) at a concentration of 3 μM to measure
154 NMDAR currents in the absence of $GABA_A$-mediated currents (Vargas-Caballero et al. 2011). To
155 measure the contribution of AMPAR and NMDAR-mediated currents to individual EPSCs, the
156 holding membrane potential was clamped at −70mV and +40mV, respectively, in alternating
157 sweeps. Cells were maintained at −70 mV in between stimuli and the membrane potential was
158 changed to holding potential 2 sec prior to synaptic stimulation. Evoked EPSCs were analysed
159 using custom-written MATLAB scripts. A minimum of 5 continuously recorded sweeps for each
160 AMPAR and NMDAR were measured. AMPAR current was measured at its peak and NMDAR
161 current was measured as the average current at 55-57ms following stimulation, at which time
162 the AMPAR showed decay to ~5% of its peak amplitude. The NMDAR/AMPAR ratio was
163 calculated by dividing the amplitude of NMDAR current measured by the peak AMPAR current.
164 Successful patch clamp recordings in whole-cell configuration could be made up until 12 hours
165 after resection using this tissue.
166
167 Averaged evoked NMDAR currents (from peak back to baseline) were fitted with least squares
168 (Matlab) using a double exponential equation as follows:
169 $I_t = I_{fast}*e^{-\tau_{fast}} + I_{slow}*e^{-\tau_{slow}}$

170 where I_{fast} and I_{slow} were the amplitudes of the fast and slow decay components, and τ_{fast} and
171 τ_{slow} are the decay time constants. Following Stocca and Vicini (1998) we used a weighted mean
172 decay time constant to compare a single experimental value across conditions:

173 $\tau_w = [I_{fast}/(I_{fast} + I_{slow})] * \tau_{fast} + [I_{slow}/(I_{fast} + I_{slow})] * \tau_{slow}$

174 A single τ_w value was obtained per patient by averaging τ_w from different cells.

175

176 Co-immunoprecipitation

177 Fresh frozen human tissue blocks immediately adjacent to sliced/fixed tissue, were stored at -
178 80°C after resection was homogenized on ice using a Pellet Pestle in SDS-free RIPA buffer (2x
179 Phosphate Buffered saline (PBS); 1% sodium deoxycholate; 1% NP40, 5mM EDTA; Halt protease
180 and phosphatase inhibitor cocktail (ThermoFisher Scientific). Homogenates were centrifuged at
181 14,000 rpm for 10 min 4°C and supernatants were collected for BCA assaying (ThermoFisher
182 Scientific) to determine protein concentrations. One lysate sample for each human case was set
183 aside for Western blotting as input lane. For immunoprecipitation, a total of 1mg of protein was
184 diluted in 1ml of RIPA buffer. A pre-clear step was performed by adding protein A-agarose beads
185 (Merck Millipore) to the lysates, while rotating for 30min at 4°C. Following centrifugation at
186 10,000 rpm for 2 min, the supernatants were collected and samples were incubated overnight at
187 4°C with PSD-95 antibody raised in rabbit (CST #2707; 1:50 dilution), or rabbit IgG as control.
188 Samples were precipitated by incubating with protein A-agarose beads for 1 hr at 4°C.
189 Precipitated proteins were released from the beads by heating at 95°C for 5 min in 4X loading
190 sample buffer prior to SDS-PAGE along with 18.75 μg of input.

191

192 SDS-PAGE and Western Blotting

193 Equal amounts of protein (28μg) were separated in 7.5% acrylamide gels by SDS-PAGE and
194 transferred onto nitrocellulose membranes. Membranes were blocked in 5% (w/v) non-fat milk
195 for 1hr at room temperature and incubated overnight at 4°C in 5% (w/v) bovine serum albumin
196 (BSA) containing 0.1% (v/v) Tween-20 and one of the following primary antibodies: anti-
197 NMDAR2A (ab133265; 1:1000; Abcam); anti-NMDAR2B (610416; 1:1000; BD Neurosciences),
198 anti-PSD-95 (D27E11; 1:1000; CST), and GAPDH (D16H11; 1:1000; CST). Membranes were
199 washed 3 times with Tris-buffered saline (TBS) containing 0.1% Tween-20 (TBS-T) and probed
200 with fluorophore-conjugated goat anti-mouse/-rabbit secondary antibody (1:10000; LI-COR).
201 Proteins were visualised using the Odyssey infrared scanner (LI-COR) and bands were quantified
202 as a proportion of housekeeping protein GAPDH using Image Studio Light Software.
203
204 Immunohistochemistry
205 Tissue was immediately fixed in 4% paraformaldehyde for 24 hrs and cut into 35 µm free-floating
206 sections for immunohistochemistry. All washes were performed with PBS containing 0.1%
207 Tween-20 (PBS-T 0.1%), unless stated otherwise. Sections were incubated in 0.3% H2O2, 10%
208 methanol in PBS-T 0.1% for 30mins and then in blocking solution containing 5% goat serum
209 (Sigma Aldrich), 5% BSA (Fisher Scientific, BP1600) in PBS-T 0.2% for 1hr. Sections were then
210 incubated overnight at 4°C in blocking solution containing one of the following primary
211 antibodies: anti-GFAP (1:2000; Merck Millipore) and anti-Iba1 (1:500; Wako). Sections were then
212 washed (3 x 5min) and incubated with the appropriate biotinylated secondary antibody (1:200,
213 Biotinylated Goat Anti-Mouse Antibody (BA-9200), 1:200, Biotinylated Goat Anti-Rabbit Antibody
214 (BA-1000), Vector Labs). Sections were then incubated in the avidin-biotinylated horseradish
215 peroxidase complex (ABC) for 30 minutes. Following the ABC incubation sections were mounted
216 onto gelatinised slides and were developed using 3,3'-diaminobenzidine (DAB) precipitation.

217 Sections were washed (3 x 5min) in 0.1M PB, dehydrated using increasing ethanol percentages
218 (70%, 80%, 95% and 2x100%, for 5 minutes each). Sections were incubated in xylene
219 (2x10minutes each) and mounted using Entellan® New, mounting medium. Images from stained
220 sections were taken using a Leica Microscope (Leica DM5000B) with Q software for image
221 capture.
222 Sections were visualised using 3,3'-diaminobenzidine (DAB) precipitation under a light
223 microscope (Leica DM5000B) with Q software for image capture. GFAP- and Iba1-positive cells
224 were counted in 12 layer II-III sampling fields per case (chosen at random from 2-3 different
225 slices) of temporal cortical tissue from putative non-pathological and pathological (sclerotic
226 hippocampus or glioma) samples with available tissue using ImageJ (NIH) software.
227

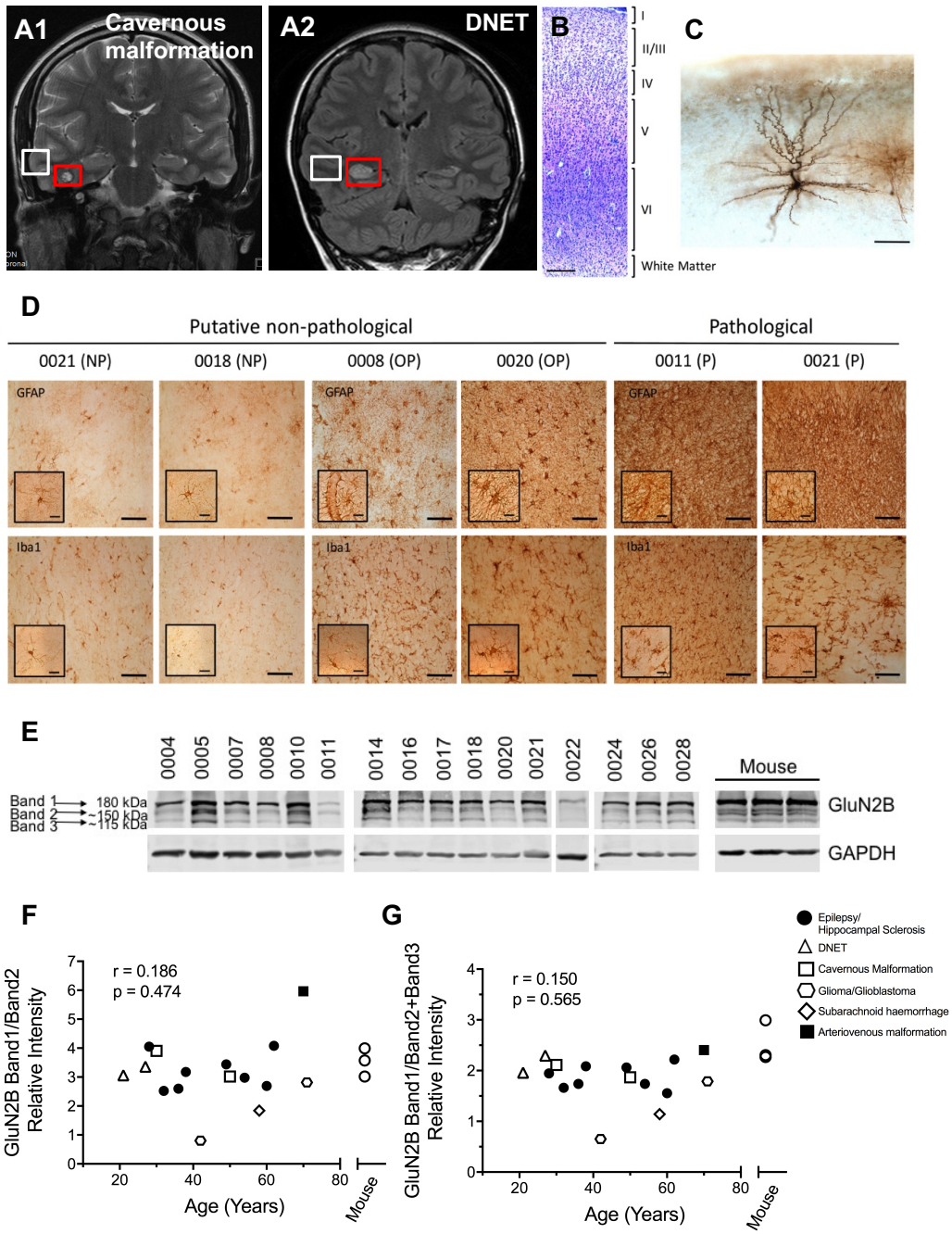

228

229 Figure 1. Characterisation of human brain tissue resected from neurosurgical cases. (A) MRI

230 images from two patients. Coronal T2 image of a cavernous malformation (A1) and coronal FLAIR

231 image of a DNET (A2) taken prior to surgery. Red box: area of pathology necessitating

232 neurosurgical removal, white box: resected tissue used for analysis. (B) Nissl stain in fixed tissue

233 showing the preservation of cortical layer architecture. (C) Visualisation of a LII-III pyramidal

234 neuron that was recorded in patch clamp mode and dialyzed with biocytin, fixed, and DAB

235 stained. (D) Immunohistochemical analysis of putative non-pathological resected tissue
236 compared with pathological tissue resected from the region of underlying pathology.
237 Representative images of immunostaining for inflammatory markers, GFAP and Iba1, of putative
238 non-pathological (PNP) resected temporal cortex showing no pathology (NP), of putative non-
239 pathological resected temporal cortex where we observed pathology (OP), and of known
240 pathological tissue, resected from the regions of underlying pathology (P). (E) GluN2B
241 immunoblot using resected human samples; lysates made from fresh-frozen human temporal
242 cortices tissue and from fresh-frozen mouse temporal cortices (n=3). (F) Band1/Band2 and (G)
243 Band1/(Band2+Band3) ratio plotted against age. No correlation observed between the ratios and
244 subject age (Spearman's coefficient of correlation (r) and p-value (p) are indicated). Scale bars in
245 (**B**) = 200 µm, in (**C**) = 100 µm, in (**D**) = 100 µm (Inset = 20 µm) . Symbols in F and G correspond to
246 the neurological condition necessitating neurosurgery.
247
248
249 **Results**
250 We used non-pathological cortical tissue samples resected during neurosurgical procedures to
251 obtain access to deep brain lesions (Fig. 1A, Table 1). The tissue was collected in theatre and
252 rapidly processed using the brain slice technique (Verhoog et al. 2013). The well-preserved
253 cortical architecture of these slices (Fig. 1B) allowed for electrophysiological recordings in
254 putative LII-III pyramidal neurons that were identified by their location within cortical layers and
255 their morphology (Fig. 1C). First, we characterised the quality and health of collected tissues
256 using fixed or snap-frozen samples of brain tissue that were immediately adjacent to that used
257 for electrophysiology. Reactive astrocytes and activated microglia are reliable inflammatory
258 indicators of disease in mammalian brain tissue (Perry et al. 2010) (Figure 1D). As positive

259 controls for inflammatory pathology, we stained pathological sections (epileptic foci N = 2
260 patients, tumour tissue N = 1 or cavernous malformation tissue N = 1) with GFAP to label
261 astrocytes and Iba1 to label microglia. We compared putative non-pathological tissue
262 (Supplementary Fig. 1A-E) against pathological tissue (cases 11 and 21). Qualitatively, the
263 putative non-pathological tissue showed normal GFAP-positive cell morphology in contrast with
264 highly ramified and fibrotic astrocytes observed in pathological tissue. Furthermore, the GFAP
265 density was significantly lower in putative non-pathological tissue than in pathological tissue. In
266 our Iba1 analyses, we found two cases with activated microglia density similar to that of positive
267 controls (Fig. 1D and Suppl. Fig. 1C). We therefore labelled these two cases as observed
268 pathology (OP) and excluded them from synaptic analyses. The density of microglia in the human
269 brain does not change with age, as recently reported by us (Askew et al. 2017). Here, we
270 observed densities in accordance with previously published data, and similarly did not observe
271 significant age-dependent changes in astrocyte density ($r = -0.03$ $p = 0.92$) or microglia density (r
272 $= -0.54$ $p = 0.09$).
273
274 Next, we sought to further control for resected tissue quality by measuring the ratio of full
275 length to cleaved GluN2B protein, which has previously been demonstrated as a robust control
276 for synaptic proteome integrity in post-mortem human brain tissue (Bayés et al. 2014). Using
277 Western blot analysis of GluN2B in fresh frozen samples with an antibody that recognises full-
278 length protein (Band 1, 180kDa) and cleaved products (Bands 2 and 3, 150 and 115kDa), we
279 measured the ratio of full-length to cleaved GluN2B (Figure 1E-G). All except one of our samples
280 met the criteria of Band 1/Band 2 ratio >1 (Bayés et al. 2014) demonstrating lack of proteome
281 degradation. Given the observed degradation of full-length GluN2B, the sample showing a ratio
282 of <1 (case 0011), was excluded from synaptic analyses. All fresh-frozen tissue samples showed

283 the presence of GluN2B cleavage products, likely indicating functional and turnover-related
284 regulation of the channel by proteases such as calpain (Wu et al. 2005). The full-length-to-
285 cleaved band ratio was not altered with age (Figure 1F-G). We observed a similar GluN2B protein
286 profile in rapidly processed adult mouse brain tissue (Fig 1E-G), which confirmed that basal
287 cleavage of GluN2B in fresh frozen tissue was not an artefact of tissue collection. This shows that
288 high quality tissue can be obtained from human patients irrespective of age.
289
290 To test whether total protein levels decrease with age, we performed further Western blot
291 quantifications of GluN2A and GluN2B subunits. We found that both GluN2A and GluN2B protein
292 levels decreased with age, and a trend ($p = 0.08$) was observed for GluN2A-S (Fig 2A-D). Using
293 PSD-95 pull-down from brain homogenates we were able to observe both GluN2A and GluN2B in
294 samples from 27, 49 and 50 year old patients, however in a sample from a 58 year old we were
295 not able to see GluN2B co-immunoprecipitated with PSD-95 (Fig 2E). Not all samples yielded
296 successful precipitated PSD-95 lanes and thus we did not quantify co-precipitation. To analyse
297 whether the observed decrease in GluN2A and GluN2B NMDAR subunits was associated with
298 overall reduction in synaptic proteins we also tested available samples for synapsin (pre-
299 synaptic), PSD-95 (post-synaptic) and the AMPAR subunit GluA1 (Fig 3A). We observed that there
300 was no significant correlation with age in the amount of these proteins in cortical homogenate
301 normalised against tubulin (Fig 3B-G) or against total protein load (Ponceau stain of Western blot
302 membrane, data not shown). However, a significant negative correlation of GluN2B protein
303 levels with age was consistently observed when normalising against tubulin (Fig 3B), Ponceu
304 stain (not shown) or against PSD-95 (Fig 3F) as a postsynaptic protein control.
305
306

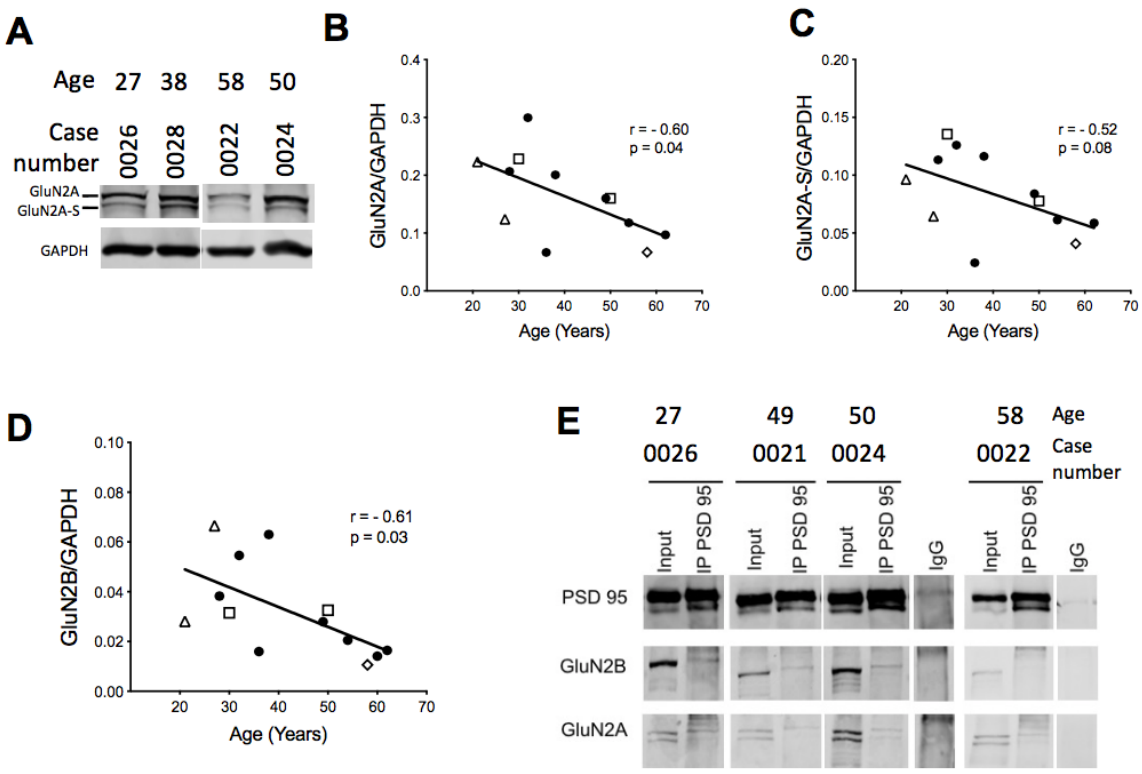

307

308

309 Figure 2. GluN2A and GluN2B protein levels in adult human temporal cortical tissue

310 homogenate show an age-dependent decline. **(A) Representative examples of GluN2A blot**

311 **showing GluN2A and GluN2A-S bands.** Quantification for GluN2A **(B)** and GluN2A-S (C), and

312 GluN2B (B, from blots shown in Fig. 1E) relative to the constitutive protein GAPDH. Spearman's

313 coefficient of correlation (r) and p-value (p) are indicated for each measure. (E) Representative

314 blots of GluN2A and GluN2B subunits co-immunoprecipitated with PSD-95 using human

315 temporal cortical tissue lysates. Symbols in B, C and D correspond to the neurological condition

316 necessitating neurosurgery as depicted in Figure 1.

317

318

319

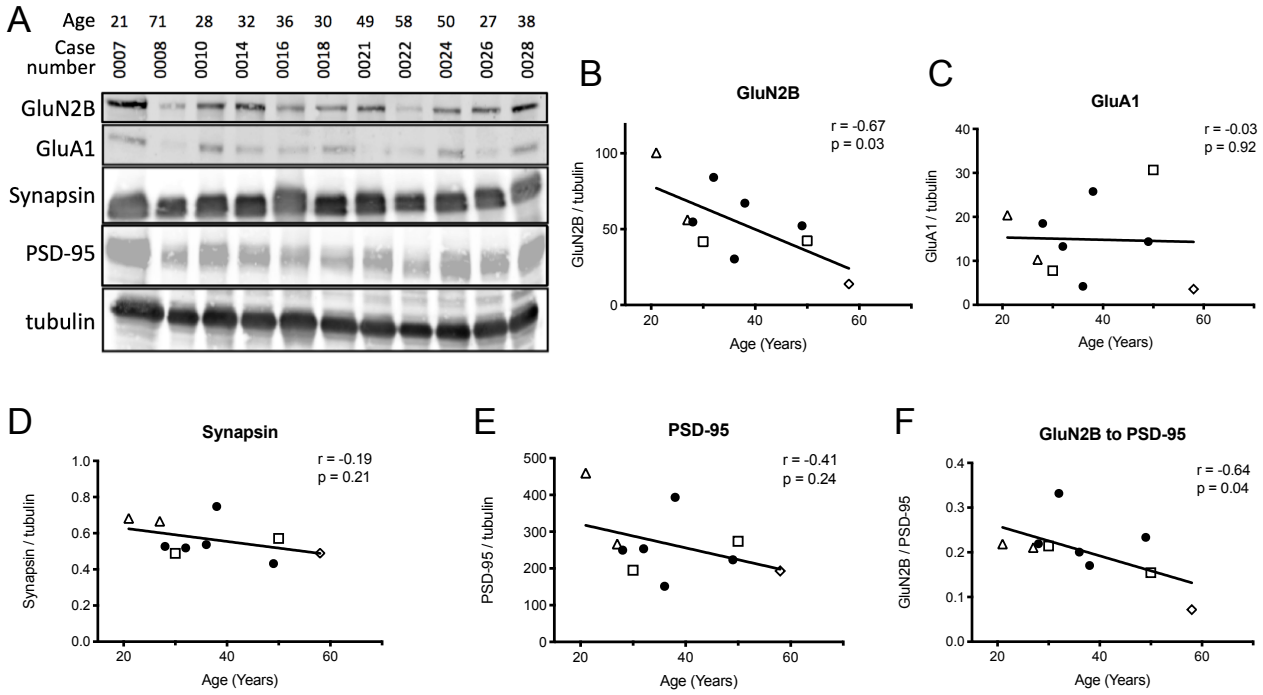

Figure 3. Age dependence of GluN2B and other synaptic protein expression in human temporal tissue homogenate (A) Western blot for GluN2B and other synaptic proteins with tubulin as loading control. Quantification of GluN2B (B), GluA1 (C), synapsin (D) and PSD-95 (E) normalised to tubulin and plotted against age. (F) Quantification of GluN2B normalised to PSD-95 (G) and plotted against age. Spearman's coefficient of correlation (r) and p-value (p) are indicated for each measure. Symbols in C-G correspond to the neurological condition necessitating neurosurgery as depicted in Figure 1. Case 0008 in (A) was pathological and was not quantified.

We next analysed patch clamp recordings to determine whether these receptors participate in basal synaptic transmission. NMDA and AMPA currents exhibited current voltage relationships similar to those observed in rodents (Figure 4A-B). We analysed the age-dependence of NMDA/AMPA receptor ratio by measuring AMPAR component at -70 mV and NMDAR component at sustained +50 mV depolarisation to relieve the Mg^{2+} block (Mierau et al. 2004; Vargas-Caballero and Robinson, 2004), in subsets of cells with and without pre-incubation with

335 the selective GluN2B inhibitor, Ro 25-6981 (500 nM), which shows similar pharmacological
336 properties in both rat and human recombinant receptors (Hedegaard et al. 2013). The
337 NMDA/AMPA ratio showed a significant decrease with age (Figure 4C), suggesting an age-
338 dependent reduced contribution of NMDARs to synaptic transmission. In contrast, the
339 NMDA/AMPA ratio remained constant across ages in recordings from slices pre-incubated with
340 Ro 25-6981 (Figure 4D), which at 500 nM inhibits recombinant NMDAR di-heteromers
341 (GluN1/GluN2B). This suggests that GluN2B loss could be a key determinant of reduced synaptic
342 NMDAR input to ageing temporal cortical synapses.
343 In a subset of experiments, NMDAR currents were measured before and after application of Ro
344 25-6981 in the same cell. These experiments required holding neurons in whole-cell
345 configuration for >30 minutes to allow time for initial dialysis of intracellular voltage-clamp
346 solution, acquisition of control data, wash in of bath-applied Ro and, importantly, to allow time
347 for full NMDAR current inhibition by the use-dependent antagonist Ro 25-6981 (Fischer et al.
348 1997). We observed that NMDA/AMPA ratios from subjects younger than 45 showed sensitivity
349 to Ro treatment while those for older than 45 subjects did not (<45 years old NMDA/AMPA ratio
350 before = 0.88 ± 0.20, after Ro 25-6981 treatment = 0.46 ± 0.05 N = 3, and >45 years old
351 NMDA/AMPA ratio before = 0.53 ± 0.15 after Ro 25-6981 treatment 0.474 ± 0.08, $p < 0.05$, N =
352 5). These data also show that the fraction of NMDAR current inhibited by Ro was larger in
353 synapses from younger individuals (42% ± 0.15 versus 1% ± 0.16 in older individuals, $p < 0.05$).
354 These findings are consistent with our results above using Ro preincubation.
355
356 Given that recombinant NMDARs containing either GluN1/GluN2A and GluN1/GluN2B have
357 distinct postsynaptic current decay kinetics (Stocca and Vicini, 1998), we fitted a double
358 exponential decay function to all recorded currents and obtained a weighted time constant value

359 (τ_w, see methods) for each case. We found that τ_w decreased significantly with age, this is
360 consistent with synapses from younger individuals having a higher proportion of synaptic GluN2B
361 containing receptors that is progressively reduced with age (Fig 4E). Interestingly, we found that
362 in the presence of Ro 25-6981 500 nM there was still significant decrease of τ_w with age albeit at
363 lower significance value ($p < 0.05$) and with a smaller correlation coefficient than in the absence
364 of Ro 25-6981 ($r = -0.57$). It is possible that tri-heteromers, that have τ_w larger than
365 GluN1/GluN2A but lower than GluN1/GluN2B di-heteromers are the cause of this enhanced τ_w in
366 younger individuals. In this instance, Ro 25-6981 (an ifenprodil derivative) would only achieve
367 partial inhibition of tri-heteromers even at saturating antagonist concentrations (Stroebel et al.
368 2018). However, we cannot rule out whether other slower-decaying NMDAR variants (e.g.
369 GluN2D or those containing GluN1-1a) are present at a younger age in human cortical synapses.
370

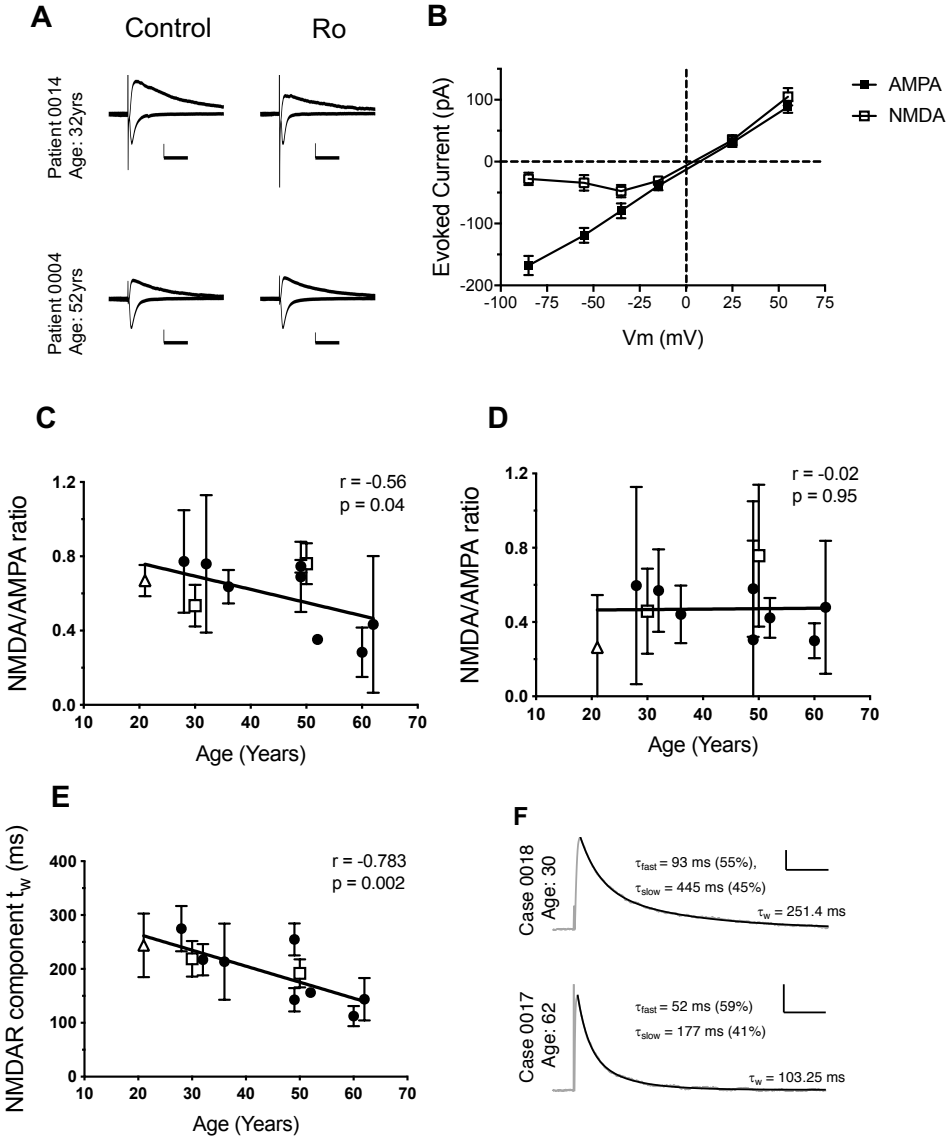

Figure 4. NMDA/AMPA responses from human cortical synapses with or without specific GluN2B inhibitor and their age dependence. (A) Representative NMDA- and AMPA-mediated currents from adult human brain slices in LII-III temporal cortex voltage clamped at -70 and +50mV with and without 500 nM Ro 25-6981 treatment. NMDAR-mediated currents from a 32-year-old are slow-decaying and with Ro treatment they producing a smaller and faster decaying outward current. NMDAR-mediated currents from a 52-year-old show no sensitivity to Ro 25-6981 treatment. (B) Average I/V relations for NMDA and AMPA responses (n=7 patients). I/V

379 relations for NMDA-mediated responses show a voltage dependence (characteristic 'J-shaped'
380 curve), showing the block of the receptor at hyperpolarized membrane potentials. I/V relations
381 for AMPA-mediated responses are linear. (C) NMDA/AMPA ratios are negatively correlated with
382 age under control conditions. (D) No correlation was observed between NMDA/AMPA ratios and
383 age for recordings carried in 500 nM Ro 25-6981. (E) The weighted NMDAR time constant τ_w
384 shows an age dependent decline, suggesting a reduced contribution of the slow decaying
385 GluN1/GluN2B containing NMDARs. Each data point represents the average measure ± SEM per
386 patient. (F) Sample lines of best fit. Scale bars in (A) = 50 ms, 50 pA and (F) = 200 ms, 50 pA.
387 Scatter dot plots with error bars in graphs represent mean ± SEM per patient. Spearman's
388 coefficient of correlation (r) and p-value (p) are indicated for each measure. Symbols in C, D and
389 E correspond to the neurological condition necessitating neurosurgery as depicted in Figure 1.
390

391 Discussion.

392 A sharp developmental increase in GluN2A and a decrease in GluN2B-containing NMDARs has
393 been observed in many model systems including rodents (Dumas, 2005; Yashiro and Philpot,
394 2009 and reviewed in Paoletti et al. 2013). In humans, an 8% reduction in *GRIN2B* mRNA
395 expression during mid-gestation was accompanied by a 21% increase in *GRIN2A* mRNA
396 expression (Bagasrawala et al. 2016), these observations are consistent with larger scale mRNA
397 analyses across the human lifespan showing that, while minor changes occur with GRIN2B during
398 embryonic development and adult life, a major increase in GRIN2A expression is observed during
399 gestation (Bar-Shira et al. 2015).

400 Although GluN2A containing channels are broadly considered the major carriers of NMDAR-
401 mediated synaptic current in the adult forebrain (Hildebrand et al. 2014), adult GluN2B-
402 containing NMDARs are required in adult brain circuits to regulate synaptic strength and
403 memory in mice. In hippocampal CA3-CA1 synapses the levels of GluN2B expression in CA3-CA1
404 synapses are correlated with the ability of synapses to undergo long term potentiation (Kohl et
405 al. 2011). The high affinity association between GluN2B subunits with CaMKIIα (Barria and
406 Malinow 2005) is hypothesised to promote localisation of this molecular Ca2+ dependent switch
407 to synaptic regions and influence nearby downstream effectors of synaptic maintenance and
408 plasticity. The long decay kinetics exhibited by GluN2B containing NMDAR can effectively
409 integrate trains of stimuli by providing a long window for coincidence detection of synaptic
410 release and post-synaptic depolarisation (Vargas-Caballero and Robinson, 2004) a function which
411 may contribute to working memory in the prefrontal cortex where a substantial fraction of
412 GluN2B-containing NMDARs remains in adulthood (Wang et al. 2008).

413

414 NMDARs are essential for numerous spatial memory tasks as well as for many forms of long-term
415 synaptic plasticity, a molecular correlate of learning and memory (Bliss and Collingridge 1993;
416 Takeuchi et al. 2013). Overexpression of the GluN2B subunit in mice led to increased recruitment
417 of synaptic GluN2B, improved performance in memory tests and enhanced synaptic plasticity
418 (Tang et al. 1999, Cui et al. 2011).
419
420 In adult and ageing rodents, the contribution of GluN2B to synaptic function is reduced
421 compared to younger animals and the decline in GluN2B subunit expression is correlated with
422 impaired memory functions (Clayton et al. 2002; Magnusson, 2012; Magnusson et al. 2010; Zhao
423 et al. 2009). However, it was not known whether age dependent changes in GluN2B synaptic
424 composition also occurred over the adult human lifespan. To analyse the age dependence of
425 NMDAR composition in human synapses we studied samples from adult patients within a broad
426 age span. Using GFAP and Iba1 as inflammation markers and GluN2B as a protein degradation
427 marker, we were able to assess the quality of this tissue as non-pathological. We observed that
428 although protein expression for both glutamate receptor subunits GluN2A and GluN2B is
429 reduced with age, both proteins are still produced at detectable levels in older adults (Fig 2). By
430 using a pharmacological approach, whereby Ro 25-6981 500 nM selectively inhibits receptors
431 containing GluN1/GluN2B subunits, our data demonstrate that a significant fraction of these
432 NMDAR channels participate in basal synaptic function in cortical slices in younger adults but less
433 so in older adults. This result is in sharp contrast with predictions from equivalent mouse studies,
434 and our own analyses where Ro 25-6981 had no significant effect of the NMDA/AMPA ratio in
435 young adult mice (3-5 months) (Supplementary Figure 2 1A-C). Thus, our data using
436 pharmacological blockade of synaptic currents with Ro 25-6981, and changes in τ_w in synaptic

437 NMDAR currents shows that synaptic GluN2B contribution is reduced in human cortical synapses
438 with ageing.
439 Mechanisms of synaptic anchoring via post-translational modifications (Lussier et al. 2015)
440 and/or association with other synaptic density proteins (Chen et al. 2015) may underlie this age-
441 dependent GluN2A or GluN2B content in human cortical synapses. Further analyses of human
442 tissue derived from neurosurgery allowing for the analysis of well-preserved protein-protein
443 interactions and post-translational modifications will allow a deeper understanding of the factors
444 that cause GluN2B loss from older human synapses. Our measures do not distinguish between
445 di-heteromeric receptors (GluN2B/GluN1) or tri-heteromeric receptors (GluN2B/GluN2A/GluN1),
446 both of which show a widespread expression adult rodent brain (Rauner and Köhr, 2011) and
447 further biochemical and/or pharmacological analysis will be required to address their
448 contribution to human cortical synaptic transmission. Our measures focused on synaptic inputs
449 to excitatory neurons, however, in rodents inhibitory interneurons also possess specific subsets
450 of synaptic glutamatergic receptors including those containing GluN2B (reviewed in Akgül et al
451 2016) which are regulated in a regional and developmental manner. Further analysis will be
452 required to test the synaptic composition in identified subtypes of human inhibitory
453 interneurons.
454
455 Mounting evidence in model systems shows that a reduction in synapse number and turnover,
456 as well as alterations of synaptic receptor composition, are correlated with age-related cognitive
457 decline in rodents and primates (Morrison and Baxter, 2012; Mostany et al. 2013). Previous
458 work suggests a causal role of GluN2B recruitment at the synapse in regulating synaptic strength
459 and memory storage. Furthermore, overexpression of the GluN2B subunit in mice led to
460 increased recruitment of synaptic GluN2B resulting in improved memory and enhanced synaptic

461 plasticity (Cui et al. 2011; Tang et al. 1999). Since synaptic NMDAR content and composition can
462 determine integrative and plastic properties in neurons (Yashiro and Philpot, 2009), our
463 observations highlight a biologically plausible mechanism for the reduction in cortical plasticity
464 observed across the human age span (Freitas et al. 2011) and the cognitive ageing in the human
465 brain which can be observed from middle age (Singh-Manoux et al. 2012).
466
467 Experiments using live human tissue derived from neurosurgery can further our understanding
468 of molecular mechanisms behind synaptic ageing synapse alterations in disease. This can be
469 studied either directly in diseased tissue from patients (Finardi et al. 2006; Ying et al. 2004) or by
470 acutely mimicking disease states using non-pathological tissue processed with the brain slice
471 technique (Vargas-Caballero et al. 2016).
472
473 Understanding synaptic composition throughout the human age span can also inform drug
474 development for neurological conditions affecting young or older individuals, as well as aid in
475 understanding and ameliorating off-target effects of widely used drugs. As an example,
476 fluoxetine (Prozac), also inhibits GluN2B-containing receptors (Kiss et al. 2012) and thus, may
477 have differential side-effects in young and older brains. Furthermore, data on human synapse
478 composition and function, such as our work presented here, can serve as a benchmark to further
479 develop pluripotent stem cell models (Zhang et al. 2016) to mimic the GluN2A/ GluN2B synaptic
480 composition for the disease model of interest.
481
482 Funding.

483 This work was supported by the Institute for Life Sciences, University of Southampton (Senior
484 Research Fellowship to MVC) and Wessex Medical Trust (Innovation Grant to MVC). CMP was
485 funded by the Gerald Kerkut Trust and the Institute for Life Sciences (PhD studentship).

486

487 Acknowledgements.

488 We thank Prof. Delphine Boche for helpful discussions on human brain tissue
489 immunohistochemistry.

490

491

492

493 References

494 Akgül G, McBain CJ. 2016. Diverse roles for ionotropic glutamate receptors on inhibitory
495 interneurons in developing and adult brain. J Physiol. 594:5471–5490.
496
497 Al-Hallaq RA, Conrads TP, Veenstra TD, Wenthold RJ. 2007. NMDA Di-Heteromeric Receptor
498 Populations and Associated Proteins in Rat Hippocampus. J Neurosci. 27:8334–8343.
499
500 Askew K, Gomez-Nicola D. 2018. A story of birth and death: Insights into the formation and
501 dynamics of the microglial population. Brain Behav Immun. 69:9-17
502
503 Bagasrawala I, Memi F, V. Radonjić N, Zecevic N. 2016. N -Methyl d-Aspartate Receptor
504 Expression Patterns in the Human Fetal Cerebral Cortex. Cereb Cortex. 11:5041-5053.
505
506 Bar-Shira O, Maor R, Chechik G. 2015. Expression Switching of Receptor Subunits in Human Brain
507 Development. PLOS Comput Biol 11:31004559.
508
509 Barria A, Malinow R. 2005. NMDA receptor subunit composition controls synaptic plasticity by
510 regulating binding to CaMKII. Neuron. 48:289–301.
511
512 Bayés A, Collins MO, Galtrey CM, Simonnet C, Roy M, Croning M, Gou G, van de Lagemaat LN,
513 Milward D, Whittle IR, Smith C, Choudhary JS, Grant S. 2014. Human post-mortem synapse
514 proteome integrity screening for proteomic studies of postsynaptic complexes. Mol Brain. 7:88.
515
516 Bliss TV, Collingridge GL. 1993. A synaptic model of memory: long-term potentiation in the

517 hippocampus. Nature. 361:31–9.

518

519 Chen X, Levy JM, Hou A, Winters C, Azzam R, Sousa AA, Leapman RD, Nicoll RA, Reese TS. 2015.
520 PSD-95 family MAGUKs are essential for anchoring AMPA and NMDA receptor complexes at the
521 postsynaptic density. Proc Natl Acad Sci. 112:E6983–E6992.

522

523 Clayton DA, Mesches MH, Alvarez E, Bickford PC, Browning MD. 2002. A hippocampal NR2B
524 deficit can mimic age-related changes in long-term potentiation and spatial learning in the
525 Fischer 344 rat. J Neurosci. 22:3628–37.

526

527 Cui Y, Jin J, Zhang X, Xu H, Yang L, Du D, Zeng Q, Tsien JZ, Yu H, Cao X. 2011. Forebrain NR2B
528 overexpression facilitating the prefrontal cortex long-term potentiation and enhancing working
529 memory function in mice. PLoS One. 6:e20312

530

531 Dumas TC. 2005. Developmental regulation of cognitive abilities: Modified composition of a
532 molecular switch turns on associative learning. Prog Neurobiol. 76:189–211.

533

534 Finardi A, Gardoni F, Bassanini S, Lasio G, Cossu M, Tassi L, Caccia C, Taroni F, LoRusso G, Di Luca
535 M, Battaglia G. 2006. NMDA receptor composition differs among anatomically diverse
536 malformations of cortical development. J Neuropathol Exp Neurol. 65:883–93.

537

538 Fischer G, Mutel V, Trube G, Malherbe P, Kew JNC, Mohacsi E, Heitz MP, Kemp JA. 1997. Ro 25-
539 6981, a Highly Potent and Selective Blocker of N-Methyl-D-aspartate Receptors Containing the
540 NR2B Subunit. Characterization in Vitro. J Pharm and Exp Ther. 283:1285–1292

541

542 Freitas C, Perez J, Knobel M, Tormos JM, Oberman L, Eldaief M, Bashir S, Vernet M, Peña-Gómez
543 C, Pascual-Leone A. 2011. Changes in cortical plasticity across the lifespan. Front Aging Neurosci.
544 3:5.

545

546 Hansen KB, Ogden KK, Yuan H, Traynelis SF. 2014. Distinct functional and pharmacological
547 properties of Triheteromeric GluN1/GluN2A/GluN2B NMDA receptors. Neuron. 81:1084–96.

548

549 Hardingham GE, Bading H. 2010. Synaptic versus extrasynaptic NMDA receptor signalling:
550 implications for neurodegenerative disorders Nature Review Neurosci. 11:682-696.

551

552 Hedegaard MK, Hansena KB, Andersena KT, Bräuner-Osborne H, Traynelis SF. 2013.
553 Molecular pharmacology of human NMDA receptors. Neurochem Int. 61:601–609.

554

555 Hildebrand ME, Pitcher GM, Harding EK, Li H, Beggs S, Salter MW. 2014. GluN2B and GluN2D
556 NMDARs dominate synaptic responses in the adult spinal cord. Sci Rep. 4:4094.

557

558 Jantzie LL, Talos DM, Jackson MC, Park H-K, Graham D a, Lechpammer M, Folkerth RD, Volpe JJ,
559 Jensen FE. 2013. Developmental Expression of N-Methyl-D-Aspartate (NMDA) Receptor Subunits
560 in Human White and Gray Matter: Potential Mechanism of Increased Vulnerability in the
561 Immature Brain. Cereb Cortex. 25:482-495.

562

563 Kiss JP, Szasz BK, Fodor L, Mike A, Lenkey N, Kurkó D, Nagy J, Vizi ES. 2012. GluN2B-containing
564 NMDA receptors as possible targets for the neuroprotective and antidepressant effects of

565 fluoxetine. Neurochem Int. 60:170–176.

566

567 Kohl MM, Shipton OA, Deacon RM, Rawlins JNP, Deisseroth K, and Paulsen O. 2013. Hemisphere-
568 specific optogenetic stimulation reveals left-right asymmetry of hippocampal plasticity. Nat
569 Neurosci. 14: 1413–1415

570

571 Lussier MP, Sanz-Clemente A, Roche KW. 2015. Dynamic Regulation of NMDA and AMPA
572 Receptors by Posttranslational Modifications. J Biol Chem. 290:28596–28603.

573

574 Magnusson KR, Brim BL, Das SR. 2010. Selective vulnerabilities of N-methyl-D-aspartate (NMDA)
575 receptors during brain aging. Front. Aging Neurosci. 2:11.

576

577 Magnusson KR. 2012. Aging of the NMDA receptor: from a mouse's point of view. Future Neurol.
578 7:627-637.

579

580 Mierau SB, Meredith RM, Upton AL, Paulsen O. 2004. Dissociation of experience-dependent and
581 -independent changes in excitatory synaptic transmission during development of barrel cortex.
582 Proc Natl Acad Sci. 101:15518–15523.

583

584 Morrison JH, Baxter MG. 2012. The ageing cortical synapse: hallmarks and implications for
585 cognitive decline. Nat Rev Neurosci. 13:240–50.

586

587 Mostany R, Anstey JE, Crump KL, Maco B, Knott G, Portera-Cailliau C. 2013. Altered Synaptic
588 Dynamics during Normal Brain Aging. J Neurosci. 33:4094–4104.

589

590 Paoletti P, Bellone C, Zhou Q. 2013. NMDA receptor subunit diversity: impact on receptor
591 properties, synaptic plasticity and disease. Nat Rev Neurosci. 14:383–400.
592

593 Perry VH, Nicoll JAR, Holmes C. 2010. Microglia in neurodegenerative disease. Nat Rev Neurol.
594 6:193–201.
595

596 Rauner C, Köhr G. 2011. Triheteromeric NR1/NR2A/NR2B receptors constitute the major N-
597 methyl-D-aspartate receptor population in adult hippocampal synapses. J Biol Chem. 286:7558–
598 66.
599

600 Singh-Manoux A, Kivimaki M, Glymour MM, Elbaz A, Berr C, Ebmeier KP, Ferrie JE, Dugravot A.
601 2012. Timing of onset of cognitive decline: results from Whitehall II prospective cohort study.
602 BMJ 344:d7622–d7622.
603

604 Stocca G, Vicini S. 1998. Increased contribution of NR2A subunit to synaptic NMDA receptors in
605 developing rat cortical neurons. J Physiol. 507:13–24.
606

607 Stroebel D, Casado M, Paoletti P. 2018. Triheteromeric NMDA receptors: from structure to
608 synaptic physiology. Curr Opin Physiol. 2:1.
609

610 Takeuchi T, Duszkiewicz AJ, Morris RGM. 2013. The synaptic plasticity and memory hypothesis:
611 encoding, storage and persistence. Philos Trans R Soc B Biol Sci. 369:20130288.
612

613 Tang YP, Shimizu E, Dube GR, Rampon C, Kerchner G a, Zhuo M, Liu G, Tsien JZ. 1999. Genetic
614 enhancement of learning and memory in mice. Nature. 401:63–69.
615
616 Vargas-Caballero M, Robinson HPC. 2004. Fast and slow voltage-dependent dynamics of
617 magnesium block in the NMDA receptor: the asymmetric trapping block model. J Neurosci.
618 24:6171–6180.
619
620 Vargas-Caballero M, Martin LJ, Salter MW, Orser BA, Paulsen O. 2010. Alpha-5 Subunit-
621 containing GABAA receptors mediate a slowly decaying inhibitory synaptic current in CA1
622 pyramidal neurons following Schaffer collateral activation. Neuropharmacology. 58:668–675.
623
624 Vargas-Caballero M, Willaime-Morawek S, Gomez-Nicola D, Perry VH, Bulters D, Mudher A. 2016.
625 The use of human neurons for novel drug discovery in dementia research. Expert Opin Drug
626 Discov. 0441:17460441.2016.1154528.
627
628 Verhoog MB, Goriounova NA, Obermayer J, Stroeder J, Hjorth JJJ, Testa-Silva G, Baayen JC, de
629 Kock CPJ, Meredith RM, Mansvelder HD. 2013. Mechanisms Underlying the Rules for Associative
630 Plasticity at Adult Human Neocortical Synapses. J Neurosci. 33:17197–17208.
631
632 Vicini S, Wang JF, Li JH, Zhu WJ, Wang YH, Luo H, Wolfe BB, Grayson DR, Otis JM, Fitzgerald MK,
633 Mueller D. 1998. Functional and Pharmacological Differences Between Recombinant N –
634 Methyl-d-Aspartate Receptors Functional and Pharmacological Differences Between
635 Recombinant N -Methyl- D -Aspartate Receptors. J Neurophysiol. 79:555–566.
636

637 Wang H, Stradtman GG, Wang XJ, Gao WJ. 2008. A specialized NMDA receptor function in layer 5
638 recurrent microcircuitry of the adult rat prefrontal cortex. Proc Natl Acad Sci. 105:16791–6.
639
640 Warming H, Pegasiou C, Pitera AP, Kariis H, Houghton SD, Kurbatskaya K, Ahmed A, Grundy P,
641 Vajramani G, Bulters D, Altafaj X, Deinhardt K, Vargas-caballero M. 2019. A primate-specific short
642 GluN2A-NMDA receptor isoform is expressed in the human brain. Molecular Brain. 12:64.
643
644 Wu HY, Yuen EY, Lu YF, Matsushita M, Matsui H, Yan Z, Tomizawa K. 2005. Regulation of N-
645 methyl-D-aspartate receptors by calpain in cortical neurons. J Biol Chem. 280:21588–93.
646
647 Yashiro K, Philpot BD. 2009. Regulation of NMDA receptor subunit expression and its implications
648 for LTD, LTP, and metaplasticity. Neuropharmacology. 55:1081–1094.
649
650 Ying Z, Bingaman W, Najm IM. 2004. Increased Numbers of Coassembled PSD-95 to NMDA-
651 receptor Subunits NR2B and NR1 in Human Epileptic Cortical Dysplasia. Epilepsia. 45:314–321.
652
653 Zhao X, Rosenke R, Kronemann D, Brim B, Das SR, Dunah a. W, Magnusson KR. 2009. The effects
654 of aging on N-methyl-d-aspartate receptor subunits in the synaptic membrane and relationships
655 to long-term spatial memory. Neuroscience. 162:933–945.
656
657 Zhang W-B, Ross PJ, Tu Y, Wang Y, Beggs S, Sengar AS, Ellis J, Salter MW. 2016. Fyn Kinase
658 regulates GluN2B subunit-dominant NMDA receptors in human induced pluripotent stem cell-
659 derived neurons. Sci Rep. 6:23837.

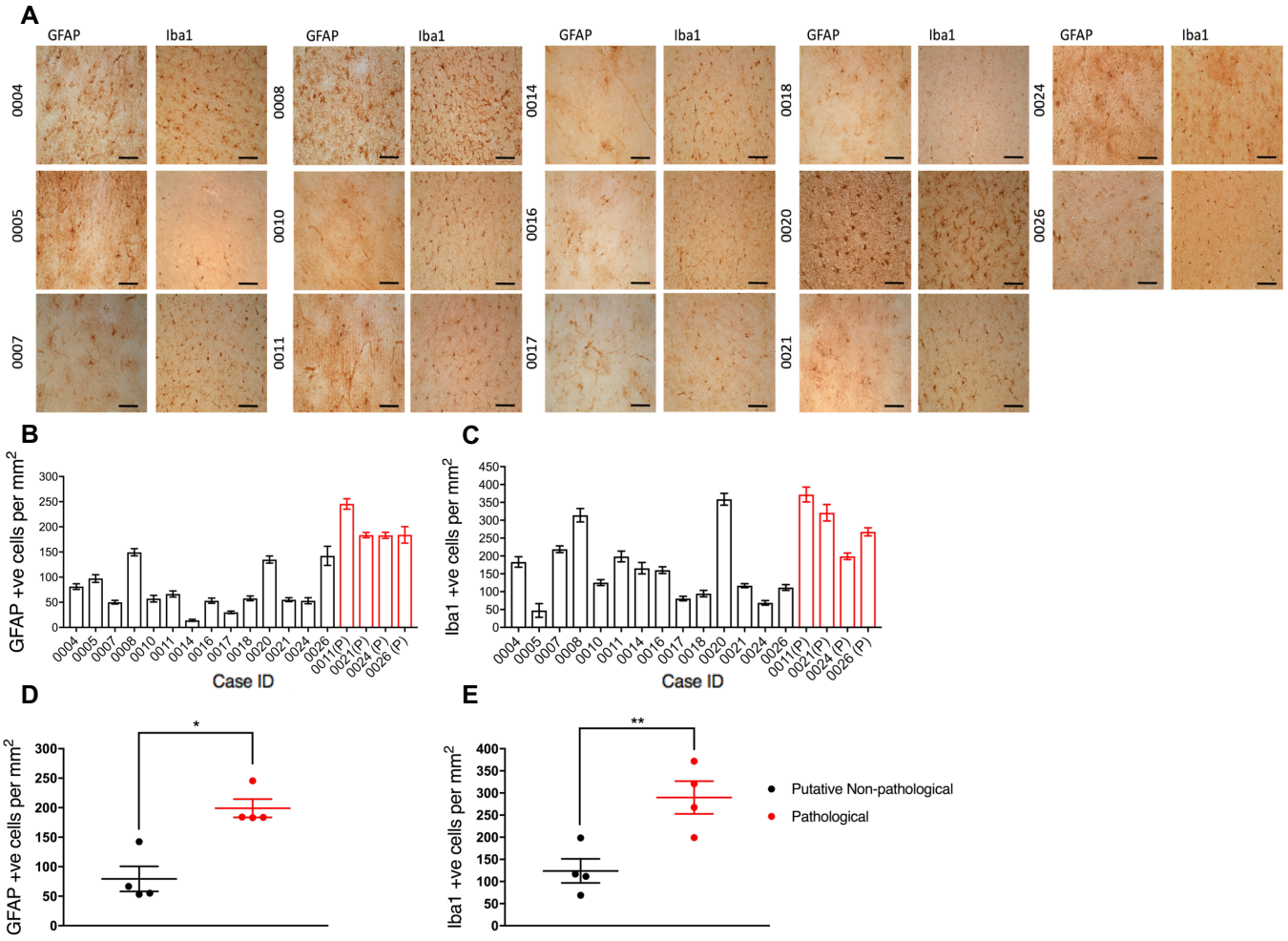

Supplementary Figure 1. Representative images of immunohistochemical analyses for cases stained for GFAP and Iba1 (A). Cell density quantification for non-pathological (PNP) and pathological (P) tissue, for GFAP (B), and Iba1 (C). Data were analysed using one-way ANOVA with Dunnett's post-hoc correction comparing against the mean of pathological cases. Cases 0008 and 0020 did not meet the criteria for subsequent analyses, as they were not significantly different to the mean of pathological cases (for Iba1). Paired comparison of cell densities for GFAP (D) and Iba1 (E) for putative non-pathological (PNP) tissue for which pathological (P) tissue was available (cases 0011, 0021, 0024 and 0026). Significantly lower densities for both GFAP and Iba1 positive cells revealed by paired t-tests (P = 0.0247 and P = 0.0018 respectively).

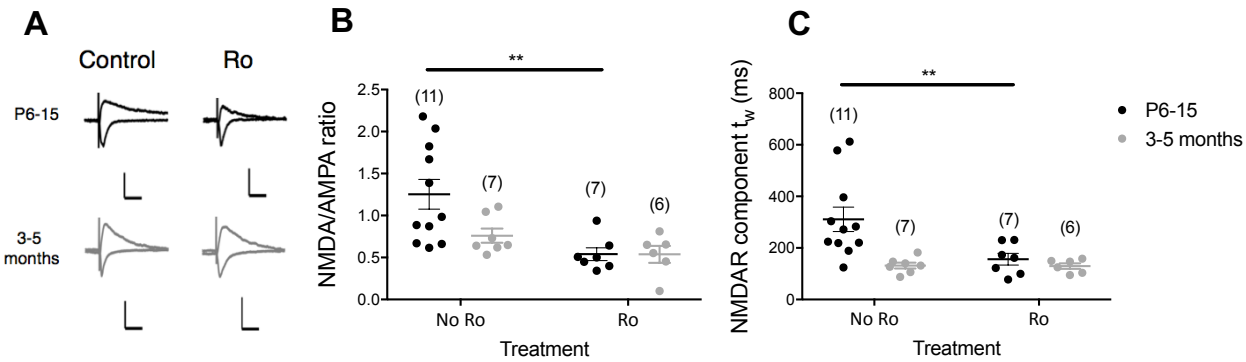

Supplementary Figure 2.

Significant GluN2B contribution in NMDA-mediated currents in temporal brain slices recorded from P6-15 mice but not from 3-5 month old (adult) mice. (A) Representative NMDAR- and AMPAR-mediated currents from P6-15 and 3- 5 month-old mice with and without Ro 25-6981 treatment. (B) NMDA/AMPA ratios from P6-15 mice show sensitivity to Ro treatment, while recordings from 3-5-month-old mice do not. (C) Weighted NMDA time constant (τ_w) shows sensitivity to Ro treatment in P6-15 mice. No differences were observed in the 3-5-month-old mice. Numbers in brackets correspond to number of cells recorded from a minimum of 4 mice. Scale bars in (A): 50ms, 100pA.